LDA+DMFT investigations of transition metal oxides and f-electron materials

Karsten Held, V. I. Anisimov, Volker Eyert, Georg Keller, A. K. McMahan, Igor Nekrasov, Dieter Vollhardt

Angaben zur Veröffentlichung / Publication details:

Held, Karsten, V. I. Anisimov, Volker Eyert, Georg Keller, A. K. McMahan, Igor Nekrasov, and Dieter Vollhardt. 2003. "LDA+DMFT investigations of transition metal oxides and f-electron materials." *Advances in Solid State Physics* 53: 267–86. https://doi.org/10.1007/978-3-540-44838-9_19.

LDA+DMFT Investigations of Transition Metal Oxides and f-Electron Materials

K. Held[1], V. I. Anisimov[2], V. Eyert[3], G. Keller[4], A. K. McMahan[5], I. A. Nekrasov[2], and D. Vollhardt[4]

[1] Max-Planck Institute for Solid State Research
D-70569 Stuttgart, Germany
[2] Institute of Metal Physics, Russian Academy of Sciences-Ural Division
Yekaterinburg GSP-170, Russia
[3] Institute for Physics, Theoretical Physics II
University of Augsburg, D-86135 Augsburg, Germany
[4] Theoretical Physics III, Center for Electronic Correlations and Magnetism
Institute for Physics, University of Augsburg
D-86135 Augsburg, Germany
[5] Lawrence Livermore National Laboratory, University of California
Livermore, CA 94550, USA

Abstract. In the last few years LDA+DMFT, the merger of conventional band structure theory in the local density approximation (LDA) with the many-body dynamical mean-field theory (DMFT) has been proven to be a powerful tool for the realistic modeling of strongly correlated electron systems. This paper provides a brief introduction to this novel computational technique and presents the results for two prime examples of strongly correlated electron systems, i.e., the Mott-Hubbard transition in V_2O_3 and the volume collapse transition in Ce.

1 Introduction

In the last century, solid state theory was divided into two main communities, the density functional [1,2,3] (DFT) band structure community, mainly based on the local density approximation (LDA), and the many-body community. The approaches developed by the respective communities are rather complementary in their strengths and weaknesses, see Table 1. LDA allows for the calculation of physical properties of real materials, starting ab initio from the potential of the ionic lattice, the kinetic energy and the Coulomb interaction of the electrons (without free parameters). Moreover, LDA calculations turned out to be unexpectedly successful, even quantitatively and even for the electronic band structure which, strictly speaking, cannot be calculated within the DFT framework. This is surprising because LDA is a serious approximation to the Coulomb interaction between electrons. In particular, the correlation but also the exchange contribution of the Coulomb interaction is only treated rudimentarily, i.e., by means of a *local* density and by a functional obtained from the jellium model [4], a weakly correlated problem. However, there are important classes of materials where LDA fails, such

Table 1. Two complementary approaches in solid state theory, pros and cons

	DFT/LDA band structure theory	many-body theory
+	• material specific (input lattice const.) no free parameters: *ab initio*	• systematic investigations of electronic correlations
	• often very successful (quantitatively)	• often allows qualitative insight
−	• effective one-particle approach fails for strong electronic correlations (transition metal oxides, f-electrons ...)	• based on model Hamiltonians (parameters needed as input)
		• CPU intensive

as transition metal oxides or heavy fermion systems, i.e., materials where electronic correlations are strong. For instance, LDA predicts La_2CuO_4 and V_2O_3, to be metals [5,6] whereas, in reality, they are insulators.

The study of the electronic correlations induced by the Coulomb interaction is the principal task of the other community, which investigates the consequential many-body physics by perturbative and non-perturbative methods. Often many-body approaches provide insight into the relevant physical mechanism. But, the electronic correlations make the theory complicated and numerical approaches CPU intensive, such that only simplified model Hamiltonians can be investigated. With the need of parameters as an input and simplified models, many-body calculations were not capable to quantitatively predict material properties. One of the most successful many-body approaches developed in the last years is the dynamical mean-field theory [7,8,9,10,11,12,13,14,15] (DMFT). This theory is controlled in the parameter $1/Z$ (Z: number of neighboring lattice sites) and reliably treats the local electronic correlations, at least for three dimensional systems. Depending on the strength of the Coulomb interaction, it yields a weakly correlated metal, a strongly correlated metal with heavy quasiparticles, or a Mott insulator. At the same time, DMFT is general and powerful enough to be applied to complicated many-body Hamiltonians.

Recently, [16,17] physicists of the two communities have joined forces to combine the advantages of LDA and DMFT and developed the computational LDA+DMFT approach which is capable of calculating strongly correlated systems such as transition metal oxides and f-electron materials realistically. In Sect. 2, we introduce this LDA+DMFT approach. Calculations for V_2O_3 and the f-electron system Ce are presented in Sect. 3 and 4, respectively. A summary closes the presentation in Sect. 5.

A more details description of LDA+DMFT can be found in [18], also see the conference proceedings [19].

2 The LDA+DMFT Approach

2.1 Local Density Approximation

Within Born-Oppenheimer approximation [20] and neglecting relativistic effects, electronic properties of solid state systems are described by the electronic Hamiltonian

$$\hat{H} = \sum_{\sigma} \int d^3r\, \hat{\Psi}^{+}(\mathbf{r},\sigma) \left[-\frac{\hbar^2}{2m_e}\Delta + V_{\text{ion}}(\mathbf{r}) \right] \hat{\Psi}(\mathbf{r},\sigma) + \frac{1}{2} \sum_{\sigma\sigma'} \int d^3r\, d^3r'\, \hat{\Psi}^{+}(\mathbf{r},\sigma)\hat{\Psi}^{+}(\mathbf{r}',\sigma')\, V_{\text{ee}}(\mathbf{r}-\mathbf{r}')\, \hat{\Psi}(\mathbf{r}',\sigma')\hat{\Psi}(\mathbf{r},\sigma). \quad (1)$$

Here, $\hat{\Psi}^{+}(\mathbf{r},\sigma)$ and $\hat{\Psi}(\mathbf{r},\sigma)$ are field operators that create and annihilate an electron at position $\mathbf{r}$ with spin σ, Δ is the Laplace operator, m_e the electron mass, e the electron charge, and

$$V_{\text{ion}}(\mathbf{r}) = -e^2 \sum_i \frac{Z_i}{|\mathbf{r}-\mathbf{R_i}|} \quad \text{and} \quad V_{\text{ee}}(\mathbf{r}-\mathbf{r}') = \frac{e^2}{2} \sum_{\mathbf{r}\neq\mathbf{r}'} \frac{1}{|\mathbf{r}-\mathbf{r}'|} \quad (2)$$

denote the one-particle ionic potential of all ions i with charge eZ_i at given positions $\mathbf{R_i}$, and the electron-electron interaction, respectively.

While the ab initio Hamiltonian (1) is easy to write down it is impossible to solve it exactly if more than a few electrons are involved. Thus, one has to do approximations. DFT/LDA turned out to be unexpectedly successful in this respect. In principle, DFT/LDA only allows one to calculate static properties like the ground state energy or its derivatives. However, in practice it turned out that the Kohn-Sham equations [2] also reliably describe the band structure [3], at least for weakly correlated materials with s and p orbitals. This corresponds to replacing the ab initio Hamiltonian (1) by

$$\hat{H}_{\text{LDA}} = \sum_{\sigma} \int d^3r\, \hat{\Psi}^{+}(\mathbf{r},\sigma) \left[\frac{-\hbar^2\Delta}{2m_e} + V_{\text{ion}}(\mathbf{r}) + \int d^3r'\, \rho(\mathbf{r}')V_{\text{ee}}(\mathbf{r}-\mathbf{r}') + \frac{\partial E_{\text{xc}}^{\text{LDA}}(\rho(\mathbf{r}))}{\partial\rho(\mathbf{r})} \right] \hat{\Psi}(\mathbf{r},\sigma). \quad (3)$$

Here, $\rho(\mathbf{r}')$ is the electron density and $E_{\text{xc}}^{\text{LDA}}(\rho(\mathbf{r}))$ the exchange correlation potential within LDA, determined by the weakly correlated jellium problem [4]. Equation (3) describes independent electrons moving in the lattice potential and the density of the other electrons, which has to be determined self-consistently.

For practical calculations one needs to expand the field operators w.r.t. a basis Φ_{ilm}, e.g., a linearized muffin-tin orbital (LMTO)[21] basis (i denotes

lattice sites; l and m are orbital indices). In this basis, one has $\hat{\Psi}^+(\mathbf{r},\sigma) = \sum_{ilm} \hat{c}^{\sigma\dagger}_{ilm} \Phi_{ilm}(\mathbf{r})$, such that the Hamiltonian (3) reads

$$\hat{H}_{\mathrm{LDA}} = \sum_{ilm,jl'm',\sigma} (\delta_{ilm,jl'm'}\, \varepsilon_{ilm}\ \hat{n}^{\sigma}_{ilm} + t_{ilm,jl'm'}\, \hat{c}^{\sigma\dagger}_{ilm} \hat{c}^{\sigma}_{jl'm'}). \tag{4}$$

Here, $t_{ilm,jl'm'} = \langle \Phi_{ilm} | -\hbar^2 \Delta/2m_e + V_{\mathrm{ion}}(\mathbf{r}) + \int d^3r' V_{\mathrm{ee}}(\mathbf{r}-\mathbf{r}')\rho(\mathbf{r}') + \partial E^{\mathrm{LDA}}_{\mathrm{xc}}(\rho(r))/\partial\rho(\mathbf{r}) | \Phi_{jl'm'} \rangle$ for $ilm \neq jl'm'$ and zero otherwise, ε_{ilm} denotes the corresponding diagonal part, and $\hat{n}^{\sigma}_{ilm} = \hat{c}^{\sigma\dagger}_{ilm} \hat{c}^{\sigma}_{ilm}$.

For d or f electrons the most important Coulomb interaction is the local Coulomb interactions on the same lattice site. These contributions are largest due to the extensive overlap (w.r.t. the Coulomb interaction) of these localized orbitals. Moreover, the largest non-local contribution is the nearest-neighbor density-density interaction which, to leading order in the number of nearest-neighbor sites, yields only the Hartree term [8,22], already included in the LDA. The large local Coulomb interactions lead to strong electronic correlations which are only very rudimentary taken into account in the LDA. To improve on this, we supplement the LDA Hamiltonian (4) with the local Coulomb matrix approximated by the (most important) matrix elements $U^{\sigma\sigma'}_{mm'}$ (Coulomb repulsion and Z-component of Hund's rule coupling) and $J_{mm'}$ (spin-flip terms of Hund's rule coupling) between the localized electrons (for which we assume $i = i_d$ and $l = l_d$):

$$\hat{H} = \hat{H}_{\mathrm{LDA}} + \frac{1}{2} {\sum_{m\sigma,m'\sigma'}}' U^{\sigma\sigma'}_{mm'} \hat{n}_{il_dm\sigma} \hat{n}_{il_dm'\sigma'}$$
$$- \frac{1}{2} {\sum_{m\sigma,m'}}' J_{mm'} \hat{c}^{\dagger}_{il_dm\sigma} \hat{c}^{\dagger}_{il_dm'\bar{\sigma}} \hat{c}_{il_dm'\sigma} \hat{c}_{il_dm\bar{\sigma}} - \sum_{m\sigma} \Delta\epsilon_d\, \hat{n}_{il_dm\sigma}. \tag{5}$$

Here, the prime on the sum indicates that at least two of the indices of an operator have to be different, and $\bar{\sigma} = \downarrow$ ($\uparrow$) for $\sigma = \uparrow$ ($\downarrow$). In typical applications we have $U^{\uparrow\downarrow}_{mm} \equiv U$, $J_{mm'} \equiv J$, $U^{\sigma\sigma'}_{mm'} = U - 2J - J\delta_{\sigma\sigma'}$ for $m \neq m'$. With M interacting orbitals, the average Coulomb interaction is then $\bar{U} = [U + (M-1)(U-2J) + (M-1)(U-3J)]/(2M-1)$. The last term of the Hamiltonian (5) reflects a shift of the one-particle potential of the interacting orbitals and is necessary if the Coulomb interaction is taken into account. This shift, the local Coulomb repulsion U, and the Hund's rule exchange can be determined by constrained LDA calculations [23].

2.2 Dynamical Mean-Field Theory

The many-body extension of LDA, Equation (5), was proposed by Anisimov et al.[24] in the context of their LDA+U approach. Within LDA+U the Coulomb interactions of (5) are treated within the Hartree-Fock approximation. Hence, LDA+U does not contain true many-body physics. While this approach is successful in describing long-range ordered, insulating states

of correlated electron systems it fails to describe strongly correlated *paramagnetic* states. To go beyond LDA+U, to capture the many-body nature of the electron-electron interaction various approximation schemes have been proposed and applied[16,17,25,26,27,28]. One of the most promising approaches, first implemented by Anisimov et al.[16], is to solve (5) within DMFT [7,8,9,10,11,12,13,14,15] ("LDA+DMFT"). Of all extensions of LDA only the LDA+DMFT approach is presently able to describe the physics of *strongly* correlated, paramagnetic metals with well-developed upper and lower Hubbard bands and a narrow quasiparticle peak at the Fermi level. This characteristic three-peak structure is a signature of the importance of many-body effects [11,12].

During the last ten years, DMFT has proved to be a successful approach for investigating strongly correlated systems with local Coulomb interactions [15]. It becomes exact in the limit of a high lattice coordination numbers Z; it is controlled in $1/Z$, [7,8] and preserves the dynamics of local interactions. Hence, it represents a *dynamical* mean-field approximation. In this non-perturbative approach the lattice problem is mapped onto an effective single-site problem which has to be determined self-consistently together with the k-integrated Dyson equation connecting the self energy Σ and the Green function G at frequency ω

$$G_{qlm,q'l'm'}(\omega) = \frac{1}{V_B} \int d^3k \left(\left[\omega 1 + \mu 1 - H^0_{\mathrm{LDA}}(\mathbf{k}) - \Sigma(\omega) \right]^{-1} \right)_{qlm,q'l'm'} . \quad (6)$$

Here, 1 is the unit matrix, μ the chemical potential, the matrix $H^0_{\mathrm{LDA}}(\mathbf{k})$ is defined as $H_{\mathrm{LDA}} - \sum_{i=i_d,l=l_d} \sum_{m\sigma} \Delta\epsilon_d \, \hat{n}_{ilm\sigma}$ with H_{LDA} being the matrix elements of (4), $\Sigma(\omega)$ denotes the self energy matrix which is non-zero only between the interacting orbitals, $[...]^{-1}$ implies the inversion of the matrix with elements n $(=qlm)$, $n'(=q'l'm')$, and the integration extends over the Brillouin zone with volume V_B.

The DMFT single-site problem depends on $\mathcal{G}(\omega)^{-1} = G(\omega)^{-1} + \Sigma(\omega)$ and is equivalent [11,12] to an Anderson impurity model if its hybridization $\Delta(\omega)$ satisfies $\mathcal{G}^{-1}(\omega) = \omega - \int d\omega' \Delta(\omega')/(\omega - \omega')$. The local one-particle Green function at a Matsubara frequency $i\omega_\nu = i(2\nu + 1)\pi/\beta$ (β: inverse temperature), orbital index m ($l = l_d$, $q = q_d$), and spin σ is given by the following functional integral over Grassmann variables ψ and ψ^*

$$G^\sigma_{\nu m} = -\frac{1}{\mathcal{Z}} \int \mathcal{D}[\psi]\mathcal{D}[\psi^*] \psi^\sigma_{\nu m} \psi^{\sigma *}_{\nu m} e^{\mathcal{A}[\psi,\psi^*,\mathcal{G}^{-1}]}. \quad (7)$$

Here, $\mathcal{Z} = \int \mathcal{D}[\psi]\mathcal{D}[\psi^*] \psi^\sigma_{\nu m} \psi^{\sigma *}_{\nu m} \exp(\mathcal{A}[\psi, \psi^*, \mathcal{G}^{-1}])$ is the partition function and the single-site action $\mathcal{A}$ has the form (the interaction part of $\mathcal{A}$ is in terms of the "imaginary time" τ, i.e., the Fourier transform of ω_ν)

$$\mathcal{A}[\psi,\psi^*,\mathcal{G}^{-1}] = \sum_{\nu,\sigma,m} \psi^{\sigma *}_{\nu m}(\mathcal{G}^{\sigma}_{\nu m})^{-1}\psi^{\sigma}_{\nu m}$$
$$-\frac{1}{2}{\sum_{m\sigma,m\sigma'}}' U^{\sigma\sigma'}_{mm'} \int_0^\beta d\tau\, \psi^{\sigma *}_m(\tau)\psi^{\sigma}_m(\tau)\psi^{\sigma' *}_{m'}(\tau)\psi^{\sigma'}_{m'}(\tau)$$
$$+\frac{1}{2}{\sum_{m\sigma,m}}' J_{mm'} \int_0^\beta d\tau\, \psi^{\sigma *}_m(\tau)\psi^{\bar{\sigma}}_m(\tau)\psi^{\bar{\sigma} *}_{m'}(\tau)\psi^{\sigma}_{m'}(\tau) \quad . \tag{8}$$

This single-site problem (7) has to be solved self-consistently together with the k-integrated Dyson equation (6) to obtain the DMFT solution of a given problem.

Due to the equivalence of the DMFT single-site problem and the Anderson impurity problem a variety of approximate techniques have been employed to solve the DMFT equations, such as the iterated perturbation theory (IPT) [11,15] and the non-crossing approximation (NCA) [29,30,31], as well as numerical techniques like quantum Monte Carlo simulations (QMC) [32], exact diagonalization (ED) [33,15], or numerical renormalization group (NRG) [34]. In principle, QMC and ED are exact methods, but they require an extrapolation, i.e., the discretization of the imaginary time $\Delta\tau \to 0$ (QMC) or the number of lattice sites of the respective impurity model $N_s \to \infty$ (ED), respectively.

In the context of LDA+DMFT we refer to the computational schemes to solve the DMFT equations discussed above as LDA+DMFT(X) where X=IPT [16], NCA [28], QMC [35] have been investigated in the case of the Sr-doped $LaTiO_3$, and quantitatively compared. [35] The same strategy was formulated by Lichtenstein and Katsnelson [17] as one of their LDA++ approaches. They also applied LDA+DMFT(IPT) [36], and were the first to use LDA+DMFT(QMC) [37], to investigate the spectral properties of iron. Recently, among others V_2O_3 [38,39], Ca(Sr)VO_3 [40], LiV_2O_4 [41], $Ca_{2-x}Sr_xRuO_4$ [42,43], CrO_2 [44], Ni [45], Fe [45], Mn [46], Pu [47], and Ce [48,49,50] have been studied by LDA+DMFT. Realistic investigations of itinerant ferromagnets (e.g., Ni) have also become possible by combining density functional theory with multi-band Gutzwiller wave functions. [51]

3 Mott-Hubbard Metal-Insulator Transition in V_2O_3

One of the most famous examples of a cooperative electronic phenomenon occurring at intermediate coupling strengths is the transition between a paramagnetic metal and a paramagnetic insulator induced by the Coulomb interaction between the electrons – the Mott-Hubbard metal-insulator transition. [52] Correlation-induced metal-insulator transitions (MIT) are found, for example, in transition metal oxides with partially filled bands near the

Fermi level. For such systems band structure theory typically predicts metallic behavior. The most famous example is V_2O_3 doped with Cr. At low temperatures, V_2O_3 is an antiferromagnetic insulator with monoclinic crystal symmetry and, at high temperature, it is a paramagnet with a corundum structure. In this paramagnetic phase, an isostructural first-order transition from a metal to an insulator occurs upon Cr-doping, accompanied by a 1-2% increase in volume. From a model point of view the MIT is triggered by a change of the ratio of the Coulomb interaction U relative to the bandwidth W. Originally, Mott considered the extreme limits $W = 0$ (when atoms are isolated and insulating) and $U = 0$ where the system is metallic. While it is simple to describe these limits, the crossover between them, i.e., the metal-insulator transition itself, poses a very complicated electronic correlation problem. Among others, this metal-insulator transition has been addressed by Hubbard in various approximations [53] and by Brinkman and Rice within the Gutzwiller approximation [54]. During the last few years, our understanding of the MIT in the one-band Hubbard model has considerably improved, in partucular due to the application of the dynamical mean-field theory [55].

Within LDA, both the paramagnetic *metal* V_2O_3 and the paramagnetic *insulator* $(V_{0.962}Cr_{0.038})_2O_3$ are found to be metallic (see Fig. 1), if one takes into account the slightly different lattice parameters [56]. The LDA DOS shows a splitting of the five Vanadium d orbitals into three t_{2g} states near the Fermi energy and two e_g^σ states at higher energies. This reflects the (approximate) octahedral arrangement of oxygen around the vanadium atoms. Due to the trigonal symmetry of the corundum structure the t_{2g} states are further split into one a_{1g} band and two degenerate e_g^π bands, see Fig. 1. The only visible difference between $(V_{0.962}Cr_{0.038})_2O_3$ and V_2O_3 is a slight narrowing of the t_{2g} and e_g^σ bands by ≈ 0.2 and 0.1 eV, respectively as well as a weak downshift of the centers of gravity of both groups of bands for V_2O_3. In particular, the insulating gap of the Cr-doped system is seen to be missing in the LDA DOS. Here we will employ LDA+DMFT(QMC) to show explicitly that the insulating gap is caused by electronic correlations. We restrict ourselves to the three t_{2g} bands at the Fermi energy and make use of a simplification for cubic transition metal oxides which allows for the use the LDA DOS instead of the full LDA Hamiltonian as an input (see [18]; note that this is an approximation for V_2O_3 since cubic symmetry is lifted).

While the Hund's rule coupling J is insensitive to screening effects and may, thus, be obtained within LDA to a good accuracy ($J = 0.93$ eV [57]), the LDA-calculated value of the Coulomb repulsion U has a typical uncertainty of at least 0.5 eV [35]. To overcome this uncertainty, we study the spectra obtained by LDA+DMFT(QMC) for three different values of the Hubbard interaction ($U = 4.5, 5.0, 5.5$ eV) in Fig. 2. From the results obtained we conclude that the critical value of U for the MIT is at about 5 eV: At $U =$ 4.5 eV one observes pronounced quasiparticle peaks at the Fermi energy,

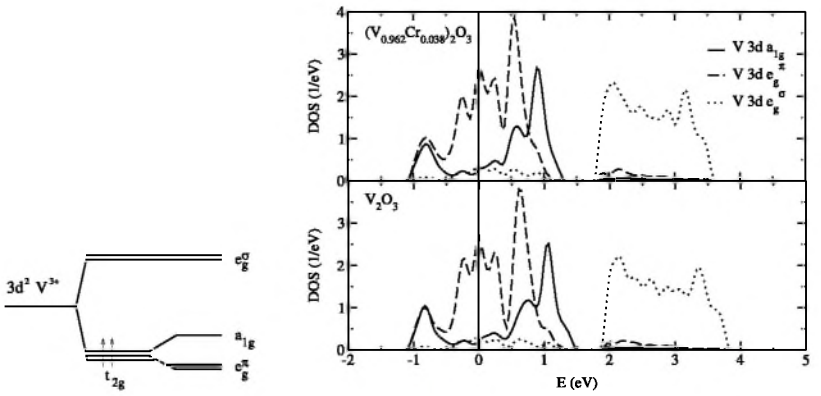

Fig. 1. *Left*: Scheme of 3*d* levels in the corundum crystal structure. *Right*: Partial LDA DOS of the 3d bands for paramagnetic metallic V_2O_3 and insulating $(V_{0.962}Cr_{0.038})_2O_3$ [reproduced from [38]]

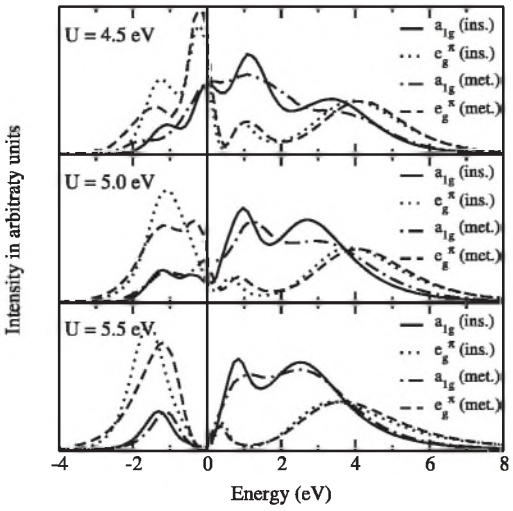

Fig. 2. LDA+DMFT(QMC) spectra for paramagnetic $(V_{0.962}Cr_{0.038})_2O_3$ ("ins.") and V_2O_3 ("met.") at $U = 4.5$, 5 and 5.5 eV, and $T = 0.1$ eV = 1160 K [reproduced from [38]]

i.e., characteristic metallic behavior, even for the crystal structure of the insulator $(V_{0.962}Cr_{0.038})_2O_3$, while at $U = 5.5$ eV the form of the calculated spectral function is typical for an insulator for both sets of crystal structure parameters. At $U = 5.0$ eV one is then at, or very close to, the MIT since there is a pronounced dip in the DOS at the Fermi energy for both a_{1g} and e_g^π orbitals for the crystal structure of $(V_{0.962}Cr_{0.038})_2O_3$, while for pure V_2O_3 one still finds quasiparticle peaks. We note that at $T \approx 0.1$ eV one only observes metallic-like and insulator-like behavior, with a rapid but smooth crossover between these two phases, since a sharp MIT occurs only at lower

temperatures [55]. The critical value of the Coulomb interaction $U \approx 5$ eV is in reasonable agreement with the values determined spectroscopically by fitting to model calculations, and by constrained LDA, see [38] for details.

To compare with the V_2O_3 photoemission spectra by Schramme et al. [58] and Mo et al. [59], as well as with the X-ray absorption data by Müller et al. [60], the LDA+DMFT(QMC) spectrum at $T = 300\,\mathrm{K}$ is multiplied with the Fermi function and Gauss-broadened by 0.09 eV to account for the experimental resolution. The theoretical result for $U = 5$ eV is seen to be in good agreement with experiment (Fig. 3). In contrast to the LDA results, our results do not only describe the different bandwidths above *and* below the Fermi energy (≈ 6 eV and $\approx 2-3$ eV, respectively), but also the position of two (hardly distinguishable) peaks below the Fermi energy (at about -1 eV and -0.3 eV) as well as the pronounced two-peak structure above the Fermi energy (at about 1 eV and 3-4 eV). In our calculation the e_g^σ states have not been included so far. Taking into account the Coulomb interaction $\bar{U} = U - 2J \approx 3\,\mathrm{eV}$ and also the difference between the e_g^σ band and the t_{2g} band centers of gravity of roughly 2.5 eV, the e_g^σ band can be expected to be located roughly 5.5 eV above the lower Hubbard band (-1.5 eV), i.e., at about 4 eV. From this estimate one would conclude the upper X-ray absorption maximum around 4 eV in Fig. 1 to be of mixed e_g^σ and e_g^π nature.

While LDA also gives two peaks below and above the Fermi energy, their position and physical origin is quite different. Within LDA+DMFT(QMC) the peaks at -1 eV and 3-4 eV are the incoherent Hubbard bands induced by the electronic correlations whereas in the LDA the peak at 2-3 eV is caused entirely by the e_g^σ (one-particle) states, and that at -1 eV is the band edge maximum of the a_{1g} and e_g^π states (see Fig. 1). Obviously, the LDA+DMFT

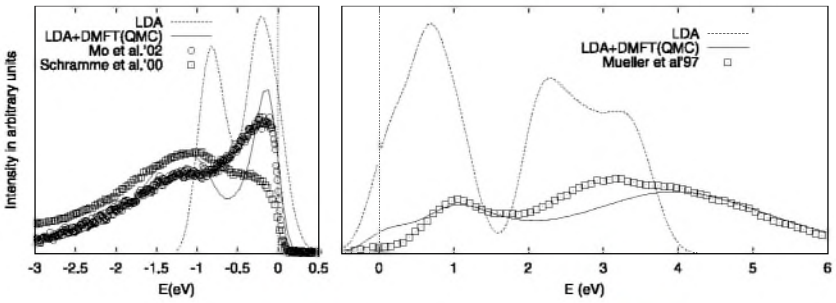

Fig. 3. Comparison of the LDA+DMFT(QMC) spectrum[38] at $U = 5\,\mathrm{eV}$ and $T = 300\,\mathrm{K}$ below (*left Figure*) and above (*right Figure*) the Fermi energy (at 0 eV) with the LDA spectrum[38] and the experimental spectrum (left: photoemission spectrum of Schramme et al. [58] at $T = 300\,\mathrm{K}$ and Mo et al. at $T = 175\,\mathrm{K}$ [59]; right: X-ray absorption spectrum of Müller et al. at $T = 300\,\mathrm{K}$ [60]). Note that Mo et al. [59] use a higher photon energy ($h\nu = 500\,\mathrm{eV}$) than Schramme et al. [58] ($h\nu = 60\,\mathrm{eV}$) which considerably reduces the surface contribution to the spectrum

results are a big improvement over LDA which, as one should keep in mind, was the best method available to calculate the V_2O_3 spectrum before.

Particularly interesting are the spin and the orbital degrees of freedom in V_2O_3. From our calculations [38], we conclude that the spin state of V_2O_3 is $S = 1$ throughout the Mott-Hubbard transition region. This agrees with the measurements of Park et al. [61] and also with the data for the high-temperature susceptibility [62]. But, it is at odds with the $S = 1/2$ model by Castellani et al. [63] and with the results for a one-band Hubbard model [64] which corresponds to $S = 1/2$ in the insulating phase and, contrary to our results, shows a substantial change of the local magnetic moment at the MIT [55]. For the orbital degrees of freedom we find a predominant occupation of the e_g^π orbitals, but with a significant admixture of a_{1g} orbitals. This admixture decreases at the MIT: in the metallic phase at $T = 0.1$ eV we determine the occupation of the (a_{1g}, e_{g1}^π, e_{g2}^π) orbitals as (0.37, 0.815, 0.815), and in the insulating phase as (0.28, 0.86, 0.86). This should be compared with the experimental results of Park et al. [61] who, from their analysis, extracted the ratio of the configurations $e_g^\pi e_g^\pi$:$e_g^\pi a_{1g}$ to be 1:1 in the paramagnetic metallic and 3:2 in the paramagnetic insulating phase. This corresponds to a one-electron occupation of (0.5,0.75,0.75) and (0.4,0.8,0.8), respectively. Although our results show a somewhat smaller value for the admixture of a_{1g} orbitals, the overall behavior, including the tendency of a *decrease* of the a_{1g} admixture across the transition to the insulating state, are well reproduced. In this context we would also like to note the work by Laad et al. [39] who started from our LDA DOS for V_2O_3 and found, within DMFT(IPT), that it is possible to trigger a Mott-Hubbard metal-insulator transition by shifting the e_g^π band with respect to the a_{1g} band.

In the study above, the experimental crystal parameters of V_2O_3 and $(V_{0.962}Cr_{0.038})_2O_3$ have been taken from the experiment. This leaves the question unanswered whether a change of the lattice is the driving force behind the Mott transition, or whether it is the electronic Mott transition which causes a change of the lattice. For another system, Ce, we will show in Section 4 that the energetic changes near a Mott transition are indeed sufficient to cause a first-order volume change.

4 Volume Collapse in Ce

Cerium exhibits a transition from the γ- to the α-phase with increasing pressure or decreasing temperature. This transition is accompanied by an unusually large volume change of 15% [65], much larger than the 1-2% volume change in V_2O_3. The γ-phase may also be prepared in metastable form at room temperature in which case the γ-α transition occurs under pressure at this temperature [66]. Similar volume collapse transitions are observed under pressure in Pr and Gd (for a recent review, see [67]). It is widely believed that these transitions arise from changes in the degree of $4f$ electron correlations,

as is reflected in both the Mott transition [68] and the Kondo volume collapse (KVC) [69] models. These two scenarios were considered to be contradictory, but might be more similar [70,71] than previously thought.

For a realistic calculation of the cerium α-γ transition, we employ the full Hamiltonian calculation where the one-particle Hamiltonian was calculated by LDA and the $4f$ Coulomb interaction U along with the associated $4f$ site energy shift [$\Delta\epsilon_d$ in Equation (5)] by a constrained LDA calculation (for details, see [67,49,50]). We have not included the spin-orbit interaction which has a rather small impact on LDA results for Ce, nor the intra-atomic exchange interaction which is less relevant for Ce as occupations with more than one $4f$-electron on the same site are rare [$J = 0$ in Equation (5)]. Furthermore, the $6s$, $6p$, and $5d$ orbitals are assumed to be non-interacting in the formalism of Equation (5). Note, that the $4f$ orbitals are even better localized than the $3d$ orbitals and, thus, uncertainties in U and the 4f site energy are relatively small and would only translate into a possible volume shift for the α-γ-transition. We would also like to note earlier calculations by Zölfl et al. [48] who studied Ce by LDA+DMFT(NCA) and by Savrasov et al. [47] who used an IPT-inspired DMFT solver for Pu.

The LDA+DMFT(QMC) spectral evolution of the Ce $4f$-electrons is presented in Fig. 4. It shows similarities to V_2O_3 (Fig. 2): At a volume per atom $V = 20\,\text{Å}^3$, Fig. 4 shows that almost the entire spectral weight lies in a large

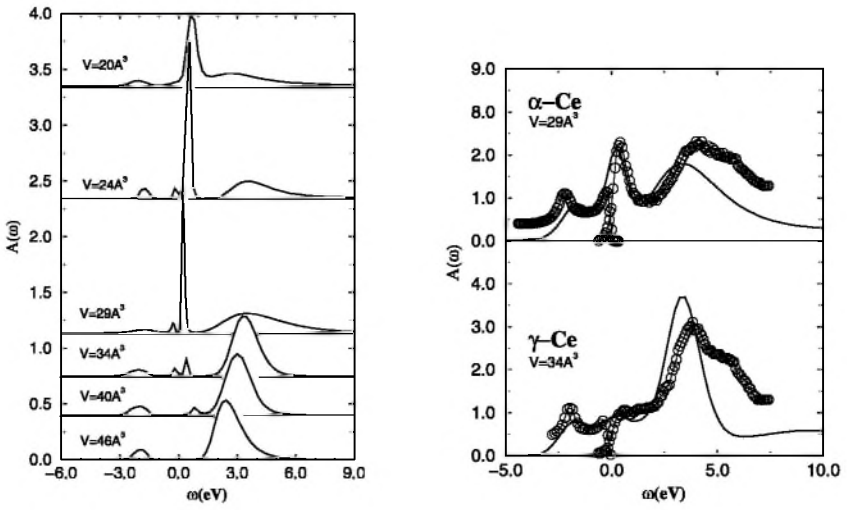

Fig. 4. *Left*: $4f$ spectral function $A(\omega)$ at different volumes and $T = 632\,\text{K}$ ($\omega = 0$ corresponds to the chemical potential; curves are offset as indicated; $\Delta\tau = 0.11\text{eV}^{-1}$); *Right*: Total LDA+DMFT *spdf*-spectrum (*solid line*) in comparison with the combined photoemission and BIS spectrum [72] (*circles*) for α-(*upper part*) and γ-Ce (*lower part*) at $T = 580\,\text{K}$ [reproduced from [50]]

quasiparticle peak with a center of gravity slightly above the chemical potential. This is similar to the LDA solution; however, a weak upper Hubbard band is also present even at this small volume. At the volumes 29 Å^3 and 34 Å^3 which approximately bracket the α-γ transition, the spectrum has a three peak structure. Finally, by $V = 46$ Å^3, the central peak has disappeared leaving only the lower and upper Hubbard bands.

In the right part of Fig. 4 we show the total LDA+DMFT *spdf*-spectrum (broadened with the experimental resolution 0.4 eV) and compare with experiment [72]. The calculated f-spectrum shows a sharp quasiparticle or Kondo resonance slightly above the Fermi energy, which is the result of the formation of a singlet state between f- and conduction states. We thus suggest that the spectral weight seen in the experiment is a result of this quasiparticle resonance. In the lower part of Fig. 4, a comparison between experiment and our calculation for γ-Ce is shown. The most striking difference between the lower and the upper part of Fig. 4 is the absence of the Kondo resonance in the γ-phase which is in agreement with our calculations. Nonetheless, γ-Ce remains metallic with spectral weight arising from the *spd*-electrons at the Fermi energy, quite contrary to V_2O_3. Altogether, one can say that the agreement with the experimental spectrum is very good, and comparable to the LDA accuracy for much simpler systems.

Fig. 5a shows our calculated DMFT(QMC) energies E_{DMFT} [49,50] as a function of atomic volume at three temperatures *relative* to the paramagnetic Hartree Fock (HF) energies E_{PMHF} [of the Hamiltonian (5)], i.e., the energy contribution due to *electronic correlations*. We also present the polarized HF energies which basically represent a (non-self-consistent) LDA+U calculation and reproduce E_{DMFT} at large volumes and low temperatures. With decreasing volume, however, the DMFT energies bend away from the polarized HF solutions. Thus, at $T = 0.054\,\mathrm{eV} \approx 600\,\mathrm{K}$, a region of negative curvature in $E_{\mathrm{DMFT}} - E_{\mathrm{PMHF}}$ is evident within the observed two phase region (arrows). Fig. 5b presents the calculated LDA+DMFT total energy $E_{\mathrm{tot}}(T) = E_{\mathrm{LDA}}(T) + E_{\mathrm{DMFT}}(T) - E_{\mathrm{mLDA}}(T)$ where E_{mLDA} is the energy of an LDA-like solution of the Hamiltonian (5) [73]. Since both E_{LDA} and $E_{\mathrm{PMHF}} - E_{\mathrm{mLDA}}$ have positive curvature throughout the volume range considered, it is the negative curvature of the correlation energy in Fig. 5a which leads to the dramatic depression of the LDA+DMFT total energies in the range $V = 26$-28 Å^3 for decreasing temperature, which contrasts to the smaller changes near $V = 34$ Å^3 in Fig. 5b. This trend is consistent with a double well structure emerging at still lower temperatures (prohibitively expensive for QMC simulations), and with it a first-order volume collapse. This is in reasonable agreement with the experimental volume collapse and strongly suggests that the electronic correlations leading to the emergence of a Kondo-like energy scale are eventually responsible for the 15% volume collapse in Ce.

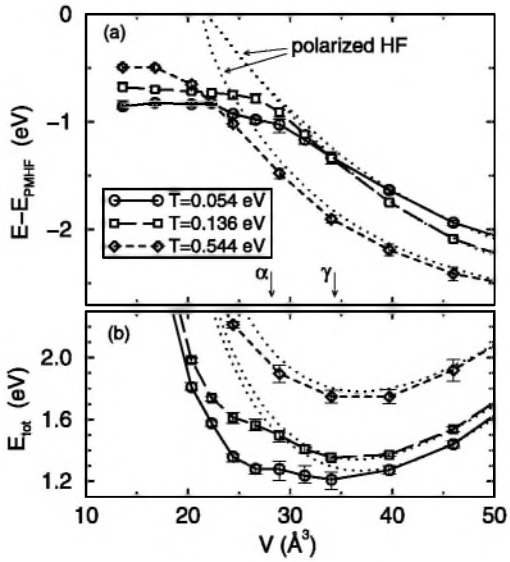

Fig. 5. (**a**) Correlation energy $E_{\mathrm{DMFT}} - E_{\mathrm{PMHF}}$ as a function of atomic volume (*symbols*) and polarized HF energy $E_{\mathrm{AFHF}} - E_{\mathrm{PMHF}}$ (*dotted lines*); *arrows:* observed volume collapse from the α- to the γ-phase. (**b**) The negative curvature of the correlation energy leads to a growing depression of the total energy near $V = 26$–28 Å^3 as temperature is decreased, consistent with an emerging double well at still lower temperatures and thus the α-γ transition. The curves at $T = 0.544$ eV were shifted downwards in (**b**) by -0.5 eV to match the energy range [reproduced from [49]]

5 Summary

In this paper we discussed the set-up of the computational LDA+DMFT scheme which merges two non-perturbative, complementary investigation techniques of solid state theory. LDA+DMFT allows one to perform ab initio calculations of real materials with strongly correlated electrons and is, at present, the only available ab initio computational technique which is able to treat systems close to a Mott-Hubbard MIT, heavy fermions, and f-electron materials.

As two particular examples we presented results for the transition metal oxide V_2O_3 and the f-electron system Ce. Our LDA+DMFT(QMC) calculations show a MIT in V_2O_3 upon Cr-doping at a reasonable value of the Coulomb interaction $U \approx 5$ eV and are in good agreement with the experimentally determined photoemission and X-ray absorption spectra for V_2O_3, i.e., above *and* below the Fermi energy. In particular, we find a spin state $S = 1$ in the paramagnetic phase, and an orbital admixture of $e_g^\pi e_g^\pi$ and $e_g^\pi a_{1g}$ configurations, which both agree with recent experiments. Thus,

LDA+DMFT(QMC) provides a remarkably accurate microscopic theory of the strongly correlated electrons in the paramagnetic metallic phase of V_2O_3.

Paramagnetic Ce undergoes an even more dramatic, isostructural volume collapse than V_2O_3. Our LDA+DMFT(QMC) spectra show a dramatic reduction in the size of the f-electron quasiparticle peak at the Fermi level when passing from the (expermental) α- to the γ-phase volume. In contrast to V_2O_3, Ce remains metallic due to the *spd* electrons. But, nonetheless, the total spectrum changes considerably and is in good agreement with experiment. An important aspect of our results is that the rapid reduction in the size of the f-electron quasiparticle peak seems to coincide with the appearance of a negative curvature in the correlation energy and a shallow minimum in the total energy. This suggest that the electronic correlations responsible for the reduction of the quasiparticle peak are associated with energetic changes strong enough to cause a volume collapse in the sense of the Kondo volume collapse model [69], or a Mott transition model [68] including electronic correlations.

Acknowledgements

We are grateful to J. W. Allen, O. K. Andersen, N. Blümer, R. Bulla, S. Horn, W. Metzner, Th. Pruschke, R. T. Scalettar, and M. Schramme for helpful discussions. We thank A. Sandvik for making available his maximum entropy code. The QMC code of [15] App. D was modified for use for some of the results of Section 4. This work was supported in part by the Deutsche Forschungsgemeinschaft through the Emmy-Noether program (KH) and Sonderforschungsbereich 484 (DV, GK, VE), the Russian Foundation for Basic Research by RFFI-01-02-17063 (VA,IN) and RFFI-02-02-06162 (IN), the Ural Branch of the Russian Academy of Sciences for Young Scientists (IN), the U.S. Department of Energy by University California LLNL under contract No. W-7405-Eng-48. (AM), the Leibniz-Rechenzentrum, München, and the John v. Neumann-Institut for Computing, Jülich.

References

1. P. Hohenberg and W. Kohn, Phys. Rev. B **136**, 864 (1964). 267
2. W. Kohn and L. J. Sham, Phys. Rev. **140**, 4A, A1133 (1965); W. Kohn and L. J. Sham, Phys. Rev. A - Gen. Phys. **140**, 1133 (1965); L. J. Sham and W. Kohn, Phys. Rev. **145 N 2**, 561 (1966). 267, 269
3. R. O. Jones and O. Gunnarsson, Rev. Mod. Phys. **61**, 689 (1989). 267, 269
4. L. Hedin and B. Lundqvist, J. Phys. C: Solid State Phys. **4**, 2064 (1971); U. von Barth and L. Hedin, J. Phys. C: Solid State Phys. **5**, 1629 (1972); D. M. Ceperley and B. J. Alder, Phys. Rev. Lett. **45**, 566 (1980). 267, 269
5. T. C. Leung, X. W. Wang, and B. N. Harmon, Phys. Rev. B **37**, 384 (1988); J. Zaanen, O. Jepsen, O. Gunnarsson, A. T. Paxton, and O. K. Andersen, Physica C **153**, 1636 (1988); W. E. Pickett, Rev. Mod. Phys. **61**, 433 (1989). 268

6. L. F. Mattheiss, J. Phys.: Cond. Matt. **6**, 6477 (1994). 268
7. W. Metzner and D. Vollhardt, Phys. Rev. Lett. **62**, 324 (1989). 268, 271
8. E. Müller-Hartmann, Z. Phys. B **74**, 507 (1989); ibid. B **76**, 211 (1989). 268, 270, 271
9. U. Brandt and C. Mielsch, Z. Phys. B **75**, 365 (1989); ibid. B **79**, 295 (1989); ibid. B **82**, 37 (1991). 268, 271
10. V. Janiš, Z. Phys. B **83**, 227 (1991); V. Janiš and D. Vollhardt, Int. J. Mod. Phys. **6**, 731 (1992). 268, 271
11. A. Georges and G. Kotliar, Phys. Rev. B **45**, 6479 (1992). 268, 271, 272
12. M. Jarrell, Phys. Rev. Lett. **69**, 168 (1992). 268, 271
13. D. Vollhardt, in *Correlated Electron Systems*, edited by V. J. Emery, World Scientific, Singapore, 1993, p. 57. 268, 271
14. Th. Pruschke, M. Jarrell, and J. K. Freericks, Adv. in Phys. **44**, 187 (1995). 268, 271
15. A. Georges et al., Rev. Mod. Phys. **68**, 13 (1996). 268, 271, 272, 280
16. V. I. Anisimov et al., J. Phys. Cond. Matter **9**, 7359 (1997). 268, 271, 272
17. A. I. Lichtenstein and M. I. Katsnelson, Phys. Rev. B **57**, 6884 (1998). 268, 271, 272
18. K. Held et al., in *Quantum Simulations of Complex Many-Body Systems: From Theory to Algorithms*, J. Grotendorst, D. Marks, and A. Muramatsu (ed.), NIC Series Volume 10, p. 175-209 (2002). 268, 273
19. A. I. Lichtenstein, M. I. Katsnelson, and G. Kotliar, to be published in *Electron Correlations and Materials Properties 2*, A. Gonis (ed.), Kluwer, New York; G. Kotliar and S. Savrasov, in *New Theoretical Approaches to Strongly Correlated Systems*, A. M. Tsvelik (ed.), Kluwer, New York, 2001, p. 259. 268
20. M. Born and R. Oppenheimer, Ann. Phys. (Leipzig) **84**, 457 (1927). 269
21. O. K. Andersen, Phys. Rev. B **12**, 3060 (1975); O. Gunnarsson, O. Jepsen, and O. K. Andersen, Phys. Rev. B **27**, 7144 (1983); O. K. Andersen and O. Jepsen, Phys. Rev. Lett. **53**, 2571 (1984). 269
22. J. Wahle et al., Phys. Rev. B **58**, 12749 (1998). 270
23. O. Gunnarson et al., Phys. Rev. B **39**, 1708 (1989). 270
24. V. I. Anisimov, J. Zaanen, and O. K. Andersen, Phys. Rev. B **44**, 943 (1991); V. I. Anisimov, F. Aryasetiawan, and A. I. Lichtenstein, J. Phys. Cond. Matter **9**, 767 (1997). 270
25. V. Drchal, V. Janiš, and J. Kudrnovský, in *Electron Correlations and Material Properties*, edited by A. Gonis, N. Kioussis, and M. Ciftan, Kluwer/Plenum, New York, 1999, p. 273. 271
26. J. Lægsgaard and A. Svane, Phys. Rev. B **58**, 12817 (1998). 271
27. Th. Wolenski, Ph.D. Thesis, Universität Hamburg 1998. 271
28. M. B. Zölfl et al., Phys. Rev. B **61**, 12810 (2000). 271, 272
29. H. Keiter and J. C. Kimball, Phys. Rev. Lett. **25**, 672 (1970); N. E. Bickers, D. L. Cox, and J. W. Wilkins, Phys. Rev. B **36**, 2036 (1987). 272
30. Th. Pruschke and N. Grewe, Z. Phys. B **74**, 439 (1989). 272
31. Th. Pruschke, D. L. Cox, and M. Jarrell, Phys. Rev. B **47**, 3553 (1993). 272
32. J. E. Hirsch and R. M. Fye, Phys. Rev. Lett. **56**, 2521 (1986); M. Jarrell, Phys. Rev. Lett. **69**, 168 (1992); M. Rozenberg, X. Y. Zhang, and G. Kotliar, Phys. Rev. Lett. **69**, 1236 (1992); A. Georges and W. Krauth, Phys. Rev. Lett. **69**, 1240 (1992); M. Jarrell, in *Numerical Methods for Lattice Quantum Many-Body Problems*, edited by D. Scalapino, Addison Wesley, 1997; for multi-band QMC,

see M. J. Rozenberg, Phys. Rev. B **55**, R4855 (1997); J. E. Han, M. Jarrell, and D. L. Cox, Phys. Rev. B **58**, R4199 (1998); K. Held and D. Vollhardt, Euro. Phys. J. B **5**, 473 (1998). 272
33. M. Caffarel and W. Krauth, Phys. Rev. Lett. **72**, 1545 (1994). 272
34. R. Bulla, Adv. Sol. State Phys. **46**, 169 (2000). 272
35. I. A. Nekrasov et al. Euro. Phys. J. B **18**, 55 (2000). 272, 273
36. M. I. Katsnelson and A. I. Lichtenstein, J. Phys. Cond. Matter **11**, 1037 (1999). 272
37. M. I. Katsnelson and A. I. Lichtenstein, Phys. Rev. B **61**, 8906 (2000). 272
38. K. Held et al., Phys. Rev. Lett. **86**, 5345 (2001). 272, 274, 275, 276
39. M. S. Laad, L. Craco, and E. Müller-Hartmann, cond-mat/0211210. 272, 276
40. I.A. Nekrasov et al., cond-mat/0211508; A. Liebsch, cond-mat/0301537. 272
41. I.A. Nekrasov et al., Phys. Rev. B **67**, 085111 (2003). 272
42. A. Liebsch and A. I. Lichtenstein, Phys. Rev. Lett. **84**, 1591 (2000). 272
43. V. I. Anisimov et al., Eur. Phys. J. B **25**, 191-201 (2002). 272
44. L. Craco, M. S. Laad, and E. Müller-Hartmann, cond-mat/0209132. 272
45. A. I. Lichtenstein, M. I. Katsnelson, and G. Kotliar, Phys. Rev. Lett. **87**, 67205 (2001). 272
46. S. Biermann et al., cond-mat/0112430. 272
47. S. Y. Savrasov, G. Kotliar, and E. Abrahams, Nature **410**, 793 (2001); S. Y. Savrasov and G. Kotliar, cond-mat/0106308. 272, 277
48. M. B. Zölfl et al., Phys. Rev. Lett. **87**, 276403 (2001). 272, 277
49. K. Held, A. K. McMahan, and R. T. Scalettar, Phys. Rev. Lett. **87**, 276404 (2001). 272, 277, 278, 279
50. A. K. McMahan, K. Held, and R. T. Scalettar, Phys. Rev. B **67**, 75108 (2003). 272, 277, 278
51. W. Weber, J. Bünemann, and F. Gebhard, in *Band-Ferromagnetism*, edited by K. Baberschke, M. Donath, and W. Nolting, Lecture Notes in Physics, Vol. 580 (Springer, Berlin, 2001), p. 9; J. Bünemann, F. Gebhard, W. Weber, Phys. Rev. B **57**, 6896 (1998). 272
52. N. F. Mott, Rev. Mod. Phys. **40**, 677 (1968); *Metal-Insulator Transitions* (Taylor & Francis, London, 1990); F. Gebhard, *The Mott Metal-Insulator Transition* (Springer, Berlin, 1997). 272
53. J. Hubbard, Proc. Roy. Soc. London Ser. A **276**, 238 (1963); **277**, 237 (1963); **281**, 401 (1964). 273
54. W. F. Brinkman and T. M. Rice, Phys. Rev. B **2**, 4302 (1970). 273
55. G. Moeller et al., Phys. Rev. Lett. **74**, 2082 (1995); J. Schlipf et al., Phys. Rev. Lett. **82**, 4890 (1999); M. J. Rozenberg, R. Chitra, and G. Kotliar, Phys. Rev. Lett. **83**, 3498 (1999); R. Bulla, Phys. Rev. Lett. **83**, 136 (1999); R. Bulla, T. A. Costi, and D. Vollhardt, Phys. Rev. B **64**, 45103 (2001); J. Joo and V. Oudovenko, Phys. Rev. B **64**, 193102 (2001); N. Blümer, Ph.D. thesis, Universität Augsburg 2002. 273, 275, 276
56. P. D. Dernier, J. Phys. Chem. Solids **31**, 2569 (1970). 273
57. I. Solovyev, N. Hamada, and K. Terakura, Phys. Rev. B **53**, 7158 (1996). 273
58. M. Schramme, Ph.D. thesis, Universität Augsburg 2000 (Shaker Verlag, Aachen, 2000); M. Schramme *et al.* (unpublished). 275
59. S.-K. Mo et al., cond-mat/0212110. 275
60. O. Müller et al., Phys. Rev. B **56**, 15056 (1997). 275
61. J.-H. Park et al., Phys. Rev. B **61**, 11 506 (2000). 276

62. D. J. Arnold and R. W. Mires, J. Chem. Phys. **48**, 2231 (1968). 276
63. C. Castellani, C. R. Natoli, and J. Ranninger, Phys. Rev. B **18**, 4945 (1978); **18**, 4967 (1978); **18**, 5001 (1978). 276
64. M. J. Rozenberg et al., Phys. Rev. Lett. **75**, 105 (1995). 276
65. *Handbook on the Physics and Chemistry of Rare Earths*, edited by K. A. Gschneider Jr. and L. R. Eyring (North-Holland, Amsterdam, 1978); in particular, D. G. Koskenmaki and K. A. Gschneider Jr., *ibid*, p.337.
66. J. S. Olsen et al., **133B**, 129 (1985). 276 276
67. A. K. McMahan et al., J. Comput.-Aided Mater. Design **5**, 131 (1998). 276, 277
68. B. Johansson, Philos. Mag. **30**, 469 (1974); B. Johansson et al., Phys. Rev. Lett. **74**, 2335 (1995). 277, 280
69. J. W. Allen and R. M. Martin, Phys. Rev. Lett. **49**, 1106, (1982); J. W. Allen and L. Z. Liu, Phys. Rev. B **46**, 5047, (1992); M. Lavagna, C. Lacroix, and M. Cyrot, Phys. Lett. **90A**, 210 (1982). 277, 280
70. K. Held et al., Phys. Rev. Lett. **85**, 373 (2000); see also C. Huscroft, A. K. McMahan, and R. T. Scalettar, Phys. Rev. Lett. **82**, 2342 (1999). 277
71. K. Held and R. Bulla, Eur. Phys. J. B **17**, 7 (2000). 277
72. L. Z. Liu et al., Phys. Rev. B **45**, 8934 (1992). 277, 278
73. We solve self-consistently for n_f using a $4f$ self energy $\Sigma = U_f(n_f - \frac{1}{2})$, and then remove this contribution from the eigenvalue sum to get the kinetic energy. The potential energy is taken to be $\frac{1}{2}U_f n_f(n_f - 1)$. 278